# FORMATION MECHANISM OF POROUS ALKALINE IRON ELECTRODES

K. VIJAYAMOHANAN* and A. K. SHUKLA

*Solid-state and Structural Chemistry Unit, Indian Institute of Science, Bangalore - 560 012 (India)*

S. SATHYANARAYANA

*Department of Inorganic and Physical Chemistry, Indian Institute of Science, Bangalore - 560 012 (India)*

(Received April 4, 1990)

## Summary

The formation mechanism of alkaline iron electrodes has been studied using galvanostatic polarisation techniques. An increase in electrode capacity is observed during initial charge–discharge cycling and is attributed to changes in the electrical conductivity, texture, and porosity of the active material. This is supported by an analysis of charge/discharge behaviour and also by linear and Tafel polarisation studies at various stages of formation. Results show that sulphide incorporation enhances the electrical conductivity and thereby exerts a beneficial effect on the charge–discharge characteristics.

## Introduction

Iron electrodes used in alkaline nickel/iron and iron/air secondary cells require several initial charge–discharge cycles at appropriate rates and temperatures to achieve a stabilized capacity. This process is conventionally called "formation cycling". Indeed, all secondary cells usually require a formation process, but this necessity, although widely acknowledged in the literature [1 - 5], has rarely been investigated in detail for iron electrodes in alkaline media.

As certain sulphide additives are known to improve the performance of porous iron electrodes in alkaline solutions [1, 4, 6], various physicochemical aspects of the electrode formation process (such as changes in the

*Author to whom correspondence should be addressed.

0378-7753/90/$3.50 

electrode texture, porosity, and bulk conductivity) are examined in this study for both sulphide-free and sulphide-modified iron electrodes. In particular, charge–discharge curves at different stages of electrode formation have been analysed, and polarisation studies on both types of electrode have been conducted in the linear and Tafel regions. These experiments have enabled a comparison to be made of the formation mechanism of sulphide-free and sulphide-modified iron electrodes.

## Experimental

Pressed-plate, porous, iron electrodes (2.8 cm × 2.4 cm × 0.1 cm) were prepared under statistically-optimized conditions, as described previously [7]. In brief, an iron–magnetite powder mixture (surface area ≃10 $m^2 g^{-1}$, particle size ≃16 $\mu$m) was obtained by thermal decomposition of ferrous oxalate. This mixture was blended with powdered graphite and polyethene, and then hot-pressed on to a nickel grid (64 mesh $cm^{-2}$). The optimum values of various parameters in the electrode fabrication were: polyethene binder = 6.5%; compaction pressure = 93.5 kg $cm^{-2}$; load retention time = 3 min; compaction temperature = 112 °C. The sulphide-modified electrodes contained 1 wt.% FeS.

The electrodes were assembled into a three-electrode cell. The latter comprised two excess-capacity nickel oxide counter electrodes, placed either side of the working electrode, and a pre-calibrated Hg/HgO, $OH^-$ (6 M KOH) reference electrode with a suitable Luggin capillary. All potentials are reported with regard to this latter electrode. The inter-electrode distance was sufficient (~2 cm) to prevent the working electrode interacting with any oxygen produced at the counter electrode. A 6 M KOH solution containing 1 wt.% LiOH was used as the electrolyte.

The capacities of the iron electrodes were measured by conducting charge ($C$/10 rate)–discharge ($C$/7 rate) cycles to a cut-off voltage of −0.80 V. This procedure corresponds to the completion of the first stage of the electrode reaction (see eqn. (1) below). In cases where the electrodes were subjected to deep discharge, the cut-off voltage was extended to −0.50 V. The temperature of the cell was maintained at 25 ± 1 °C. Steady-state, galvanostatic polarisation studies in the linear and Tafel regions were conducted on iron electrodes at various stages of formation. In order to avoid hysteresis in the linear-polarisation studies, currents were restricted to 10 $\mu$A $cm^{-2}$.

During initial charge–discharge treatment, an electrode was considered to be "formed" when the capacity did not differ by more than 5% between consecutive cycles. In order to observe the features associated with the second stage of the discharge, some of the formed electrodes were subjected to deep discharge to −0.50 V, and subsequent overcharge for 20 h at the $C$/10 rate.

## Results and discussion

An iron electrode usually undergoes a two-stage reaction during its charge–discharge process in alkaline media. Stage I corresponds to the reaction:

$$Fe + 2OH^- \longrightarrow Fe(OH)_2 + 2e^- \quad (1)$$

while stage II involves:

$$Fe(OH)_2 + OH^- \longrightarrow FeOOH + H_2O + e^- \quad (2)$$

and/or

$$3Fe(OH)_2 + 2OH^- \longrightarrow Fe_3O_4 + 4H_2O + 2e^- \quad (3)$$

Stage II is normally shorter than stage I [8 - 11]. Recent studies [12 - 14] report the final product to be mainly magnetite. During cycling, a gradual conversion of FeOOH to $Fe_3O_4$ is also possible through the reaction:

$$Fe + 8FeOOH \longrightarrow 3Fe_3O_4 + 4H_2O \quad (4)$$

The empirical open-circuit potential (OCP) for an iron electrode undergoing reaction (1) is $-0.964 \pm 0.004$ V. By comparison, the thermodynamic potential at 25 °C in 6 M KOH, after activity corrections*, is $-0.968$ V. The observed difference in OCP can be attributed to factors such as variations in the state-of-charge (SOC), the depth-of-discharge (DOD), and the amount of overcharge applied in the previous cycle. Under these conditions, the hydrogen evolution reaction:

$$2H_2O + 2e^- \longrightarrow H_2 + 2OH^- \quad (5)$$

has a thermodynamic potential of $-0.932$ V. As iron has a low hydrogen overpotential [17], the hydrogen evolution can occur even at open circuit, and the resulting potential is likely to be a mixed potential. The observed [16] invariance of the OCP with de-aeration eliminates the possibility of any significant contribution arising from the oxygen reduction reaction. Furthermore, the measured OCPs are close to the thermodynamic value for reaction (1), but are shifted about 40 mV cathodic to the thermodynamic potential for reaction (5). It is therefore reasonable to conclude that at these potentials the hydrogen evolution reaction occurs in the Tafel region, with the iron electrode reaction occurring quasi-reversibly. This conclusion is supported by the fact that the exchange current density for reaction (1) is higher than that for reaction (5) [6, 16]. Consequently, the OCP of an iron electrode in alkaline solution is a corrosion potential [18, 19].

Winkler [20] was the first to highlight the significance of the formation of iron electrodes; he established that, with cycling, the length of discharge

*This potential is calculated from the relationship, $E_r = E_r^\circ - (0.0592/2) \log [H_2O]$ with the activity of water taken as 0.559 for 6 M KOH [15]; a value of $-0.975$ V, estimated with $[H_2O] = 1$, is reported by Micka and Rousar [12].

step I increases at the expense of step II. Subsequently, formation has been considered to be an important pre-requisite in fabricating iron electrodes for alkaline secondary batteries [3 - 5]. Whilst only 3 - 5 charge–discharge cycles are sufficient for formation in the case of sintered iron electrodes, the pressed types may require more than 25 cycles, depending on the composition of the active material and the conditions of the electrode formation [3, 4, 21].

As discussed by Falk and Salkind [22], the main objectives of electrode formation are: to remove impurities, to loosen particles within the pores, to increase lattice defects, and to increase the surface area of the active material. The electrode texture is thus modified to the desired working conditions prior to its assembly in a battery. In practice, however, a deep charge–discharge cycle (100% DOD) is usually sufficient to remove any undesired impurity present in the substrate. Equally, the generation of lattice defects can be achieved within a few cycles. It is obvious, therefore, that these two factors do not dictate the formation of pressed-plate, porous, iron electrodes. In this case, other factors pertaining to the electrode morphology are likely to play a vital role in the formation process. It appears that a significant feature is the spatial evolution of an optimum porous skeleton that is capable of accommodating the drastic volume changes ($V_{ox}/V_{red}$ = 26.43 cm$^3$ mol$^{-1}$/7.11 cm$^3$ mol$^{-1}$ = 3.72) occurring in the active material during charge–discharge cycling without obstructing the access of electrolyte. Factors such as increase in mechanical strength, as well as improvement in both the electrical conductivity and the surface area of the electrode, are equally important. Besides, the dissolution–precipitation processes, involving various mobile soluble species, could bring about a redistribution of the active material and thus affect the surface morphology. A microscopic examination of the accompanying morphological changes requires an *in situ* study, but this is difficult to perform.

Figure 1 shows the variation in capacity with formation cycles for sulphide-modified and sulphide-free iron electrodes. During cycling, the DOD has been kept constant by limiting the discharge to stage I. It can be seen that the capacity of the sulphide-modified electrode, after a decrease during the second and third cycles, increases monotonically during subsequent cycling and stabilizes at ~300 mA h g$^{-1}$ after 25 cycles. By contrast, the sulphide-free electrodes, after attaining maximum capacity in about 6 - 8 cycles, exhibit a monotonic decline in capacity. This behaviour has been reported previously by Novakovskii *et al.* [11].

The decrease in the capacity of iron electrodes of either type during the second and third cycles can be explained on consideration of the studies of Silver and Lekhas [10], and of Fantgoff and Lishanskii [21]. The X-ray diffraction patterns of $Fe(OH)_2$ prepared by reducing FeOOH exhibit a greater dispersion and disorder than those of $Fe(OH)_2$ prepared by the oxidation of Fe. The discharge of the electrode subsequent to its first charge converts all available Fe to $Fe(OH)_2$, together with a small amount of FeOOH. During the following charge, the mass may not be transformed in

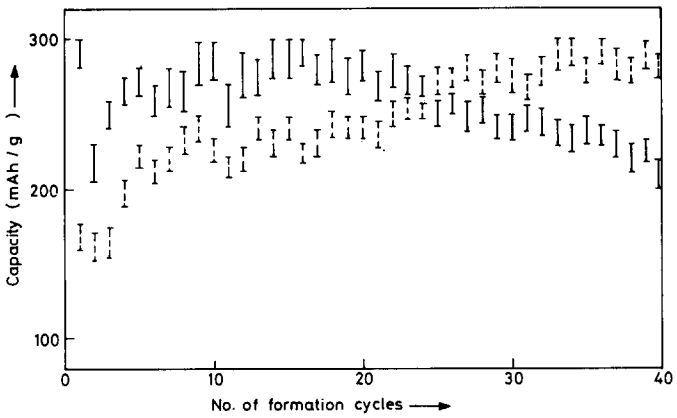


Fig. 1. Capacity of active material during formation cycling for sulphide-free (solid line) and sulphide-modified (broken line), porous, iron electrodes. Vertical lines indicate spread of data for five electrodes of each type.

its entirety to active iron, *i.e.*, part of the $Fe(OH)_2$ could become converted to $Fe_3O_4$ through the reaction:

$$4Fe(OH)_2 \longrightarrow Fe_3O_4 + Fe + 4H_2O \quad (6)$$

In subsequent cycles, the depth of electrolyte penetration into the active material increases slowly inside the pores so that more and more Fe diffuses to the electrode surface and then becomes available for electrochemical reaction, thus increasing the capacity. The higher capacity values observed for the sulphide-free electrodes during the initial 20-or-so formation cycles, compared with those for sulphide-modified electrodes, may be attributed either to a sulphide film or to a strong adsorption of sulphide ions that leach out and redistribute during further cycling. The subsequent decrease in the capacity of the sulphide-free electrodes is possibly due to an accumulation of $Fe(OH)_2$ which slowly passivates the electrode surface. On the other hand, the capacity of the sulphide-modified electrode increases due to a depassivation effect [1]. The fluctuations seen in the capacity values are possibly caused by changes in temperature and current distribution within the pores of the electrode; such fluctuations have been observed by Cnobloch *et al.* [5].

The time dependence of the OCP after termination of the charging process (SOC $\simeq$ 1) and of the closed-circuit potential after initiating a constant-current discharge ($C/10$) are shown in Figs. 2 and 3, respectively, for both the sulphide-free and the sulphide-modified electrodes during, and subsequent to, formation. The data show that the initial drop in potential arising from $I(R_{ct} + R_{ohm})$, where $R_{ct}$ and $R_{ohm}$ are the charge-transfer and ohmic resistances of the electrode, varies with the formation cycles. This is in agreement with the results of linear-polarisation experiments discussed later. It should be noted that the initial potential drop, both prior to, and after the formation, is smaller for the sulphide-modified- than for the

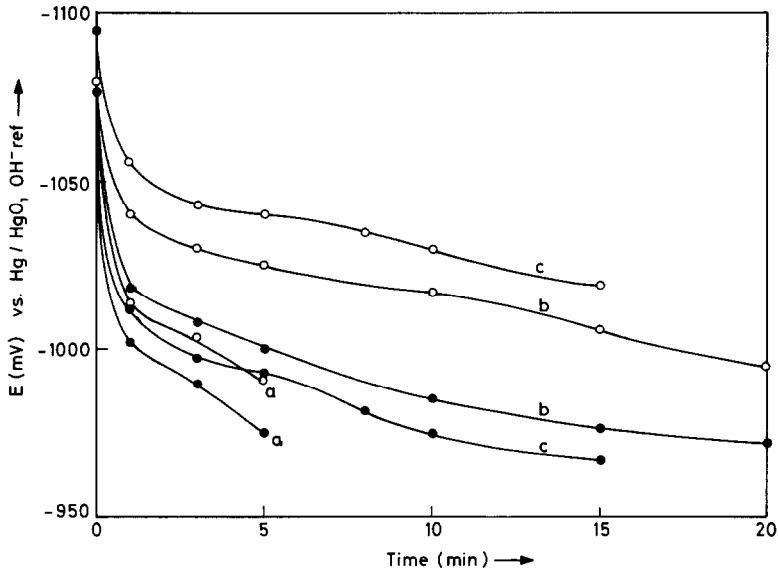


Fig. 2. Time dependence of OCP after termination of charging (SOC $\simeq$ 1) for sulphide-free (○) and sulphide-modified (●) porous, iron electrode at various formation cycles. a, b, and c correspond to cycles 2, 7, and 14, respectively.

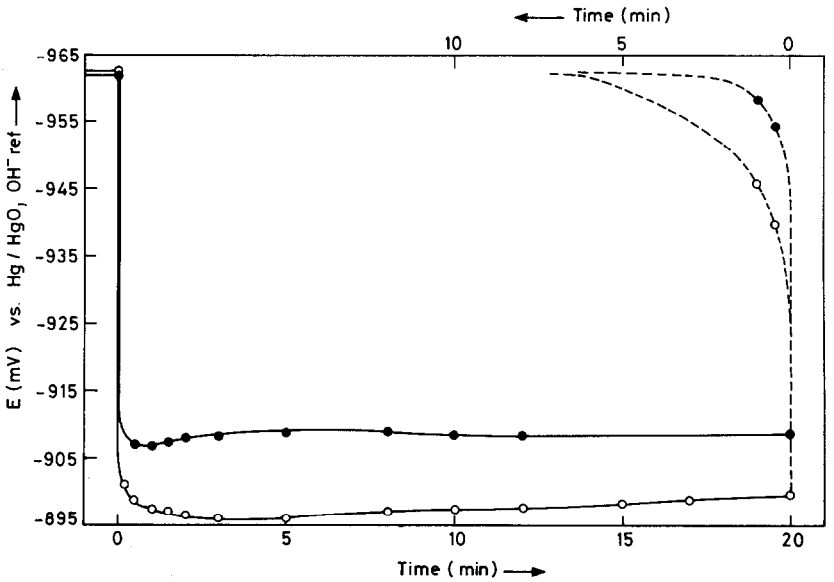


Fig. 3. Time dependence of OCP potential after initiating (——) and interrupting (- - - -) constant-current discharge for sulphide-free (○) and sulphide-modified (●) porous, iron electrodes after formation.

sulphide-free electrodes. A detailed analysis of the open-circuit transients of these two types of electrode has been described elsewhere [23] and the corresponding kinetic parameters have been accordingly evaluated.

The difference, $\Delta E$, between the open-circuit and closed-circuit potentials at the fifth minute of the respective transients for the sulphide-modified and sulphide-free electrodes is plotted as a function of cycle number in Fig. 4. It is evident that sulphide-modified electrodes exhibit less polarisation. Such an effect is also reflected in the capacity variation of the electrodes during the formation process (see Fig. 1). From the data in Fig. 4, it can be concluded that the electronic conductivity of the porous electrode, which is inversely proportional to the initial drop in potential, is higher for the sulphide-modified iron electrodes.

Figure 5(a) and (b) presents the charging patterns ($C/10$ rate) during formation of sulphide-free and sulphide-modified iron electrodes, respectively. Since the major changes in electrode capacity occur mostly within the first 15 cycles (see Fig. 1), these patterns have been compared with the corresponding charging curve on the 25th cycle for a completely formed electrode. The first charging curve exhibits a peak between −1.055 and −1.070 V for the sulphide-free iron electrode, but not for the sulphide-modified electrode. Curiously, this peak is present for sulphide-modified electrodes in subsequent cycles, but disappears for sulphide-free electrodes. Therefore, the origin of this peak appears to be different for the two types of electrode. As cycling proceeds, a shoulder corresponding to the separation of the hydrogen evolution reaction develops. This feature is clearly reflected in the charging patterns obtained for the fully formed electrodes. The end-of-charge voltage is lower for the sulphide-modified electrodes and increases with the number of cycles. This reflects the electrocatalytic effects of the sulphide additive on the hydrogen-evolution reaction [18].

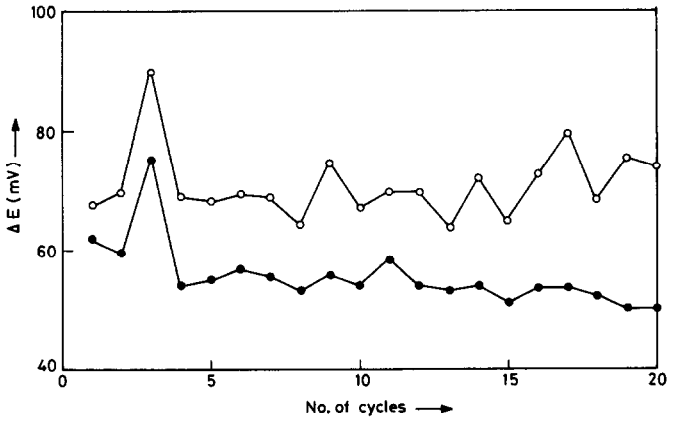


**Fig. 4. Difference between open-circuit and closed-circuit potentials (after 5 min) during discharge as a function of formation cycles for sulphide-free (○) and sulphide-modified (●) porous, iron electrodes.**

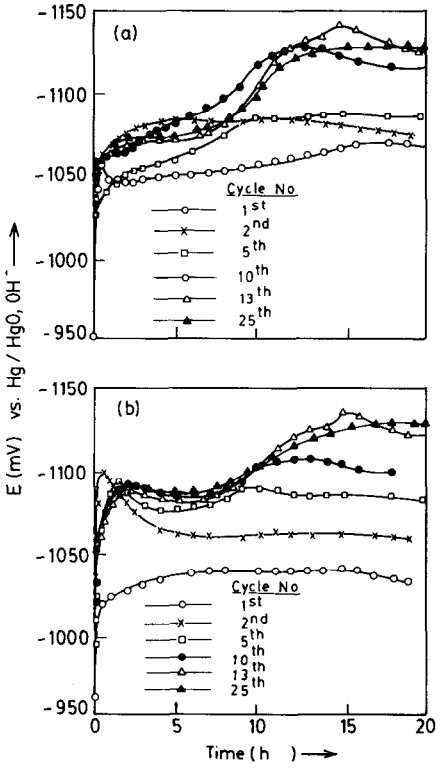


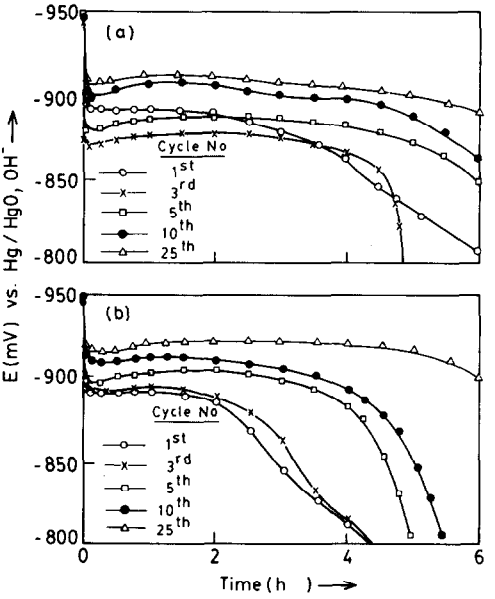


Fig. 5. Charging curves for (a) sulphide-free, and (b) sulphide-modified porous, iron electrodes during formation.

Fig. 6. Discharge curves for (a) sulphide-free, and (b) sulphide-modified porous, iron electrodes during formation.

The discharge patterns for the sulphide-free and sulphide-modified electrodes during formation are given in Fig. 6(a) and (b), respectively. The curves tend to flatten with cycling. A comparison with the respective patterns at the 25th cycle shows that the active material evolves into a suitable texture and morphology with a clear emergence of the first and second stages as formation progresses.

The results of the linear-polarisation studies conducted on sulphide-modified and sulphide-free electrodes during, and after, formation are presented in Fig. 7. The SOC value has been chosen to be $\simeq 1$ on the basis of the electrode capacity during the preceding cycle. The slopes of these curves close to the origin indicate that the sulphide-modified electrodes always exhibit a lower charge-transfer resistance.

Galvanostatic polarisation data in the Tafel region for sulphide-modified and sulphide-free electrodes at SOC $\simeq 1$ obtained during the formation cycling (Fig. 8) exhibit features that are not consistent with linear

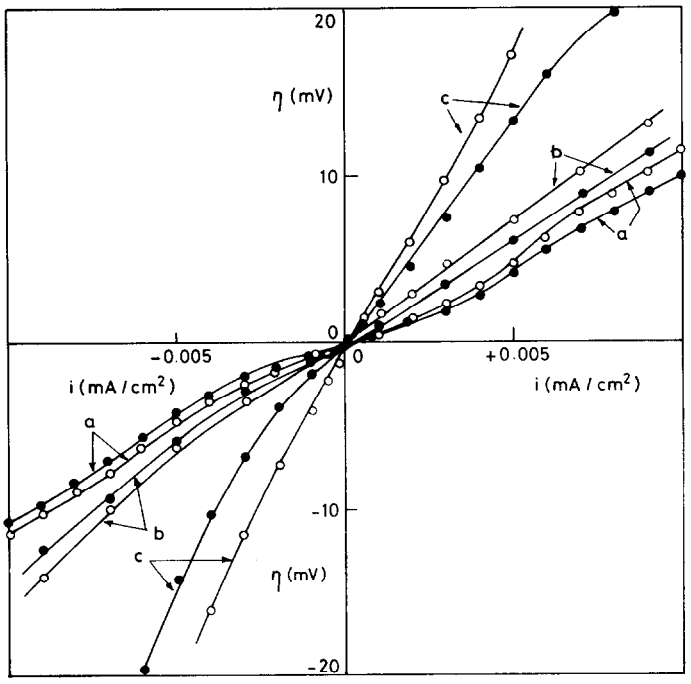


Fig. 7. Linear polarisation curves for sulphide-free (○) and sulphide-modified (●) porous, iron electrodes at SOC ≃ 1 during formation; a, b, and c correspond to cycles 2, 7, and 30, respectively.

polarisation data. Unlike the cathodic polarisation curves, the anodic polarisation curves tend to become more reversible with cycling.

A simple physical model which can account for the above experimental features is that, in the initial state, a pressed-plate, porous, iron electrode not only has a highly developed surface but also has a high density of surface defects that facilitate the hydrogen evolution reaction during polarisation. In other words, during the initial formation cycles most of the charging current is consumed by the hydrogen evolution reaction and the subsequent discharge yields only a low capacity with regard to the iron electrode reaction: $Fe + 2OH^- \rightarrow Fe(OH)_2 + 2e^-$. The electrocatalytic effects of the hydrogen evolution reaction on the porous iron electrode is reflected by the relatively low polarisation resistance in the linear polarisation curves, and also by the relatively high degree of reversibility exhibited in the Tafel plots. With an increase in the number of formation cycles, the electrocatalytic sites for the hydrogen evolution reaction on the electrode surface are either leached out or obliterated by surface/bulk diffusion, etc., thus leading to an increase in: (a) the observed polarisation resistance (now characteristic of the iron-electrode charging reaction) in the linear polarisation curves; (b) the degree of irreversibility of the cathodic Tafel curves; (c) the degree of reversibility of the anodic Tafel curves (now arising due to the iron-electrode discharge reaction).

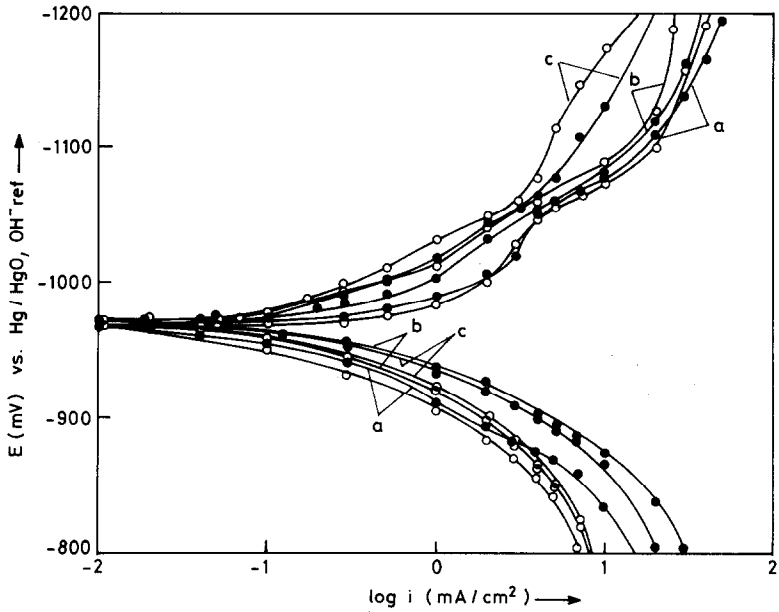


Fig. 8. Steady-state galvanostatic polarisation curves for sulphide-free (○) and sulphide-modified (●) porous, iron electrodes during formation; a, b, and c correspond to cycles 5, 15, and 25, respectively.

## Conclusions

It is suggested that the formation process provides a porous electrode with a surface texture having a relatively low electrocatalytic activity towards the hydrogen evolution reaction (the unwanted side reaction), thereby increasing the charge efficiency of the desired iron-electrode reaction. In addition, formation increases the electrical conductivity of the active material. The advantage of the sulphide modification is manifest in an optimal interfacial adsorption of sulphide ions and/or their incorporation into the electrode lattice.

## Acknowledgement

Financial assistance from the Department of Non-conventional Energy Sources, Government of India, New Delhi, is gratefully acknowledged.

## References

1 G. Berger and F. Haschka, in L. J. Pearce (ed.), *Power Sources 11*, The Paul Press Ltd., London, 1987, p. 237.

2 R. Bonnaterre, R. Doisnean, M. C. Petit and J. P. Stervinous, in J. Thomson (ed.), *Power Sources 8*, Academic Press, London, 1978, p. 249.
3 E. R. Bowerman, *Proc. 22nd Annu. Power Sources Conf., 1968*, PSC Publications, NJ, 1969, p. 70.
4 K. Micka and Z. Zabransky, *J. Power Sources, 19* (1987) 315.
5 H. Cnobloch, D. Groppel, D. Kuhl, W. Nippe and G. Siemen, in J. Thomson (ed.), *Power Sources 5*, Academic Press, London, 1975, p. 261.
6 K. Vijayamohanan, A. K. Shukla and S. Sathyanarayana, *J. Electroanal. Chem.* (in press).
7 K. Vijayamohanan, A. K. Shukla and S. Sathyanarayana, *Indian J. Technol., 24* (1986) 430.
8 A. J. Salkind, C. J. Venuto and S. U. Falk, *J. Electrochem. Soc., 111* (1964) 493.
9 T. K. Teplinskaya, N. N. Ferodova and S. A. Rozentsevig, *Zh. Fiz. Khim., 38* (1964) 2176.
10 H. G. Silver and E. Lekas, *J. Electrochem. Soc., 117* (1970) 5.
11 A. M. Novakovskii, S. A. Grushkina and R. L. Kozlova, *Zh. Prikl. Khim., 46* (1973) 2026.
12 K. Micka and I. Rousar, *Electrochim. Acta, 29* (1984) 1411.
13 I. A. Dibrov, S. M. Cheroyak-Voronich, T. V. Grigoreva and G. M. Kazlova, *Elektrokhimiya, 16* (1980) 461.
14 C. S. Tong, S. D. Wang, Y. Y. Wang and C. C. Wan, *J. Electrochem. Soc., 129* (1982) 1173.
15 R. Barnard, C. F. Randell and F. L. Tye, *J. Appl. Electrochem., 10* (1980) 109.
16 T. S. Lee, *J. Electrochem. Soc., 118* (1971) 1278.
17 K. Vijayamohanan, A. K. Shukla and S. Sathyanarayana, unpublished results, 1990.
18 I. A. Shoshina, G. S. Aleksandrova, A. L. Rotinyan and A. N. Nefyodov, *Elektrokhimiya, 21* (1985) 1552.
19 L. Ojefors, *Electrochim. Acta, 21* (1976) 263.
20 H. Winkler, *Electrochim. Acta, 3* (1960) 123.
21 V. M. Fantgoff and L. M. Lishanskii, *Elektrokhimiya, 18* (1982) 647.
22 S. U. Falk and A. J. Salkind, *Alkaline Storage Batteries*, Wiley, New York, 1969, p. 79.
23 K. Vijayamohanan, A. K. Shukla and S. Sathyanarayana, *J. Power Sources, 21* (1987) 53.